IOP Conf. Series: Journal of Physics: Conf. Series **862** (2017) 012004 doi:10.1088/1742-6596/862/1/012004

Spin-analyzed SANS for soft matter applications

W.C. Chen[1,2], J.G. Barker[1], R. Jones[1], K.L. Krycka[1], S.M. Watson[1], C. Gagnon[1,2], T. Perevozchivoka[1], P. Butler[1], T.R. Gentile[1]

[1] National Institute of Standards and Technology, Gaithersburg, Maryland 20899, USA
[2] University of Maryland, College Park, Maryland 20742, USA

E-mail: wcchen@nist.gov

Abstract.

The small angle neutron scattering (SANS) of nearly Q-independent nuclear spin-incoherent scattering from hydrogen present in most soft matter and biology samples may raise an issue in structure determination in certain soft matter applications. This is true at high wave vector transfer Q where coherent scattering is much weaker than the nearly Q-independent spin-incoherent scattering background. Polarization analysis is capable of separating coherent scattering from spin-incoherent scattering, hence potentially removing the nearly Q-independent background. Here we demonstrate SANS polarization analysis in conjunction with the time-of-flight technique for separation of coherent and nuclear spin-incoherent scattering for a sample of silver behenate back-filled with light water. We describe a complete procedure for SANS polarization analysis for separating coherent from incoherent scattering for soft matter samples that show inelastic scattering. Polarization efficiency correction and subsequent separation of the coherent and incoherent scattering have been done with and without a time-of-flight technique for direct comparisons. In addition, we have accounted for the effect of multiple scattering from light water to determine the contribution of nuclear spin-incoherent scattering in both the spin flip channel and non-spin flip channel when performing SANS polarization analysis. We discuss the possible gain in the signal-to-noise ratio for the measured coherent scattering signal using polarization analysis with the time-of-flight technique compared with routine unpolarized SANS measurements.

Key words: SANS polarization analysis, soft matter samples, spin-incoherent scattering, inelastic scattering, polarized ^{3}He, ^{3}He NSF

1. Introduction

Over the last three decades, small-angle neutron scattering (SANS) has been a powerful probe for determining the size, shape, distribution, inter- and intra-structures of particles or aggregates, such as colloidal particles, surfactant aggregates, and polymers, often existing in soft condensed matter and biology. For hydrogen-rich soft matter, hydrogen containing molecules yield a great deal of nuclear spin-incoherent scattering during SANS measurements. In order to determine the weak coherent scattering that carries the structural information of the sample, it is necessary to subtract out the nuclear spin-incoherent (NSI) background accurately, which is typically independent of the wave vector transfer Q . However, the subtraction can be challenging because accurate knowledge of the amount of this nearly Q-independent background is critical, particularly at high Q where the coherent scattering is much weaker than the background [1]. An over or under-estimation of the spin-incoherent background may change the slope of the scattering power law at high Q and thus lead to a different structural interpretation.


Content from this work may be used under the terms of the Creative Commons Attribution 3.0 licence. Any further distribution of this work must maintain attribution to the author(s) and the title of the work, journal citation and DOI.
Published under licence by IOP Publishing Ltd

Polarization analysis is a powerful technique to separate nuclear coherent scattering from magnetic scattering or to separate coherent scattering from nuclear spin-incoherent scattering [2]. Polarization analysis in SANS has been developed at the National Institute of Standards and Technology using ^{3}He neutron spin filters (NSFs) [3, 4, 5, 6] and has recently been employed for hard condensed matter investigations such as magnetic nanoparticles [7], an exchanged-biased system [8], a ferroelectric material [9], and a giant magnetostrictor [10]. SANS polarization analysis has been demonstrated for separation of coherent and incoherent scattering in special soft matter samples [3, 11, 12, 13]. For soft matter samples, typically there is no magnetic scattering. For hydrogen, two-thirds of NSI single scattering occurs in the spin-flip (SF) channel and one-third occurs in the non-spin flip (NSF) channel, resulting in a two-to-one ratio of spin-flip scattering to non-spin flip scattering in the total spin-incoherent scattering if multiple scattering is negligible. However, multiple scattering in many samples reduces the two-to-one ratio to nearly one. The measured non-spin-flip signal contains both coherent scattering and $\frac{1}{3}$ to $\frac{1}{2}$ of the total NSI scattering. In addition there is a significant amount of inelastic scattering in light water [14, 15]. For a typical sample thickness, more than 50 % of the scattering is inelastic, as shown in Table 6 in Ref. [15]. This inelastic scattering appears at a much different wavelength compared to the elastic scattering. Therefore the polarizing efficiency and transmission for the inelastic part are different from the elastic part due to the strong wavelength-dependence of the ^{3}He analyzer. Moreover, the inelastic scattering mixes with the nuclear spin-incoherent scattering, making it impossible to be separated in the current SANS polarization analysis method [3, 4]. So the presence of the inelastic scattering makes separation of the coherent and incoherent scattering incorrect.

In this paper, we report the development of SANS polarization analysis in conjunction with the time-of-flight technique using a chopper to effectively remove the inelastic scattering background. The paper is organized as following. In Sec. 2 we present a brief description of the ^{3}He NSFs and their polarized neutronic properties. In Sec. 3, we describe the polarized beam setup. In Sec. 4, we describe a general scheme of how polarized SANS data can be reduced for soft matter applications. We discuss the polarized beam calibration and time-dependence performance in Sec. 5. We present how separation of coherent and incoherent scattering can be done in combination with determination of the effective spin flip efficiency due to a multiple scattering effect in Sec. 6 and we summarize the paper in Sec. 7.

2. Polarized ^{3}He spin filter as a spin analysis device

A ^{3}He NSF is a transmission-based neutron-polarizing device. It relies upon the strong neutron spin dependent absorption cross section for ^{3}He gas via the resonance reaction ^{3}He(n,p)^{3}H. The absorption cross section $\sigma_+ = \sigma_{\uparrow\uparrow} \approx 0$ when the neutron spin is parallel to the ^{3}He spin, while $\sigma_- = \sigma_{\downarrow\uparrow} = 10666$ b at 1.8 Å when the neutron spin is anti-parallel to the ^{3}He spin. The transmission through an unpolarized beam for two neutron spin states is given by

$$T^{\pm} = T_{\rm E}\exp\left[-\sigma(\lambda)nl\left(1 \mp P_{\rm He}\right)\right] \quad (1)$$

where $T^{\pm}$ is the transmission with neutron spin parallel (+) or antiparallel (−) to the ^{3}He spin. $T_{\rm E}$ is the transmission of the glass windows of the ^{3}He cells that are fabricated from GE-180 glass [16]. $T_{\rm E}$ is typically 0.87. $P_{\rm He}$ is the ^{3}He polarization. $\sigma(\lambda)nl$ is the opacity (gas thickness) of the cell, linearly proportional to the ^{3}He gas density, the wavelength, and the length of the cell. The transmission for an unpolarized neutron beam passing through a polarized ^{3}He cell is then given by

$$T_{\rm n} = T_{\rm E}\exp\left(-\sigma(\lambda)nl\right)\cosh\left(\sigma(\lambda)nlP_{\rm He}\right) = T_0\cosh\left(\sigma(\lambda)nlP_{He}\right) \quad (2)$$

where T_0 is the transmission for an unpolarized neutron beam passing through a unpolarized ^{3}He cell.

3. Experiment setup

The experiments were performed at the National Institute of Standards and Technology Center for Neutron Research on the NG-3 SANS beam-line as shown in Fig. 1a. The SANS instrument is equipped with an V-shape Fe/Si supermirror in a transmission geometry for polarizing the incident neutrons. A precession coil spin flipper is placed immediately after the polarizer with a flipping efficiency of ϵ. A ^{3}He analyzer with a capability of inverting ^{3}He polarization online was used to spin-analyze the scattered beam from the sample. The 2-dimensional position sensitive detector on NG-3 SANS has 128 by 128 array of pixels with a pixel resolution of 5 mm. An in-house-built chopper was located directly in front of the sample. The chopper-sample assembly was placed between a pair of longitudinal coils that were used to provide a sample field of 2.3 mT and define the neutron spin axis at the sample. The chopper had a weakly magnetic rotation shaft near the neutron beam that might depolarize the incident neutron spins (see Sec. 5). However we optimized the field of the longitudinal coils to minimize neutron depolarization from the magnetic shaft. Between the chopper and the neutron guide, we placed a $\frac{\pi}{2}$ spin rotation device that was able to adiabatically rotate the neutron spin from vertical to longitudinal direction along the beam path.

The sample was comprised of 0.5 mm-thick silver behenate powder and 1 mm-thick light water (H_2O). The silver behenate powder was loaded inside a 1.43 cm diameter cadmium aperture between single layers of scotch tape (we estimated to be 0.05 mm thick in total). Light water was loaded in a quartz cell with a window thickness of 2 mm and placed directly behind the powder. SANS measurements were performed at room temperature. The sample to detector distance was set to be 2.88 m to observe the first order diffraction peak of silver behenate at 0.1076 Å^{-1}. We chose a wavelength of 7.5 Å to enhance the separation between the inelastic and elastic time-of-flight (TOF) spectrum. To extend the momentum transfer range and be able to observe the first diffraction peak at 0.1076 Å^{-1} of the silver behenate sample, the ^{3}He analyzer cell was offset to the beam center by 3.5 cm. The chopper spun a four-slot (15 degree opening) disk and operated at 2200 rpm with a duty cycle of 16.7 %. Elastic scattering from a 1 mm thick glassy carbon sample was used to characterize the time-of-flight spectrum showing that inelastic data were stripped from data files by eliminating all events having a time shorter than 4 ms, corresponding to a wavelength of 5.8 Å. The elastic data were extracted out with all events having a time longer than 4 ms. So we had the option of either using or removing the inelastic data for polarization efficiency correction and data analysis.

During the experiment, the ^{3}He polarization was maintained in a compact, magnetically shielded solenoid [17] that is 25 cm in diameter and 35 cm long. The field of the solenoid was parallel to the sample field. For the experiment, ^{3}He gas was polarized offline in one of the NIST SEOP systems [18], then transported to the NG-3 SANS beam-line. The nuclear spin-polarized ^{3}He starts to decay with time once the lasers were turned off. The ^{3}He cells we chose have an intrinsic longitudinal relaxation time of 400 h. The ^{3}He polarization relaxation time was reduced from 400 h to 225 h due to an overall volume-average transverse field gradient of $|\vec{\nabla}B_\perp/B|\approx 5.4\times10^{-4}$ cm^{-1} from the stray field of the guide field, but is still long compared to the one-hour counting time. The ^{3}He cell was placed about 25 cm away from the sample to maximize the Q range for this study and under vacuum to reduce air scattering. The ^{3}He cell used for this test has a diameter of 10 cm, covering a maximum scattering angle of $2\theta = 11$ degrees. With a larger ^{3}He cell and different setup at 5 Å, we can cover a maximum scattering angle up to 18 degrees in the future.

The neutron transmissions on the main beam were measured with and without the ^{3}He cell in the beam to determine the ^{3}He polarization. SANS measurements were done with both the chopper and the ^{3}He analyzer in the beam. Polarized beam calibration was done by measuring the four spin-dependent transmissions on the main beam (see Sec. 5). For all measurements, the data were corrected for background and the time dependence of the ^{3}He polarization was

corrected for polarized beam calibration.

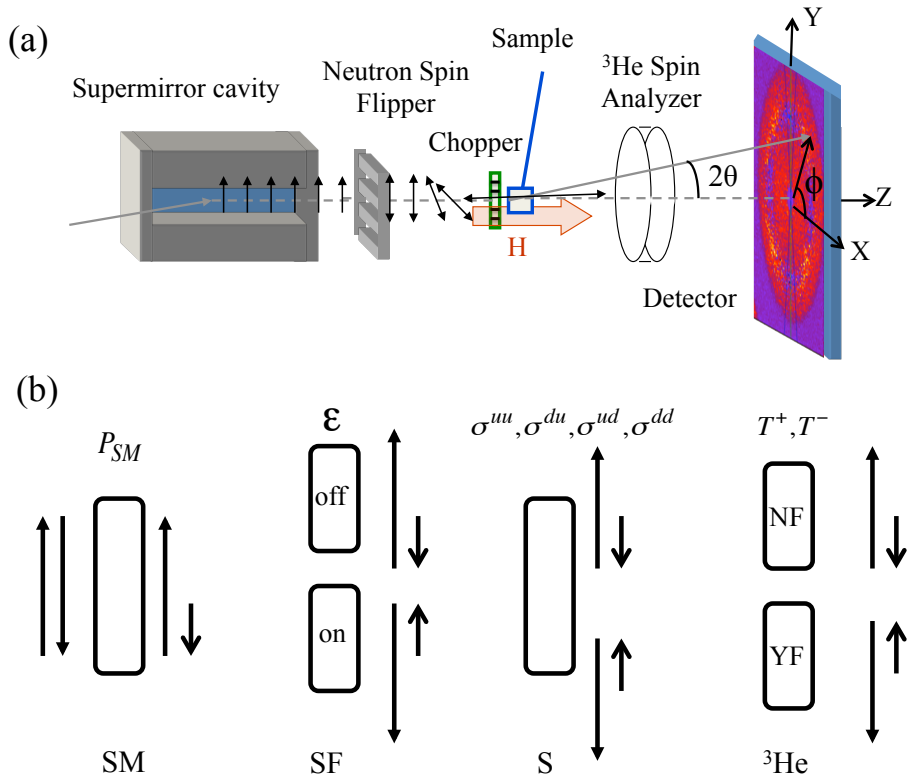

Figure 1. Color online. Schematic diagram of (a) polarized SANS setup (not to scale) with longitudinal polarization analysis and (b) possible neutron spin configurations after each polarizing element. The key instrument components shown in (a) from left to right are supermirror cavity polarizer, spin flipper, chopper and ^{3}He analyzer. An adiabatic $\frac{\pi}{2}$ spin rotation is necessary to rotate the neutron spin from the vertical direction to along the beam path between the spin flipper and chopper. The length of the arrows in (b) mimics the number of neutrons in either spin UP or DOWN. Although the neutron spins lie along the beam path in both the sample and the ^{3}He analyzer location, in the spin configuration illustration in (b), we draw them vertically for simplicity. The setup starts with a unpolarized beam. The supermirror polarizer (SM) has a polarizing efficiency of $P_{\rm SM}$. The neutron spin flipper (SF) has a flipping efficiency of ϵ. The ^{3}He analyzer (^{3}He) transmits neutrons with polarization in the same direction as that produced by the SM polarizer when not flipped (NF) or in the antiparallel direction as that produced from the SM polarizer when flipped (YF). Neutron transmissions through a ^{3}He analyzer, T^+ or T^- are defined in the text. The four possible spin-dependent scattering cross sections from the sample are defined as $\sigma^{\rm uu}$,$\sigma^{\rm du}$, $\sigma^{\rm ud}$, and $\sigma^{\rm dd}$.

4. data reduction

In this section, we describe how data reduction can be done for the spin-analyzed SANS data. The data reduction procedure has been described for hard matter samples [4]. For some magnetized samples, it is necessary to measure four spin dependent scattering cross sections. Here it is only necessary to measure two spin dependent scattering cross sections. Here we describe a simplified procedure for soft matter samples. In addition, inelastic scattering is accounted for in the polarization efficiency correction procedure. Fig. 1b shows all possible spin

configurations after each polarizing device. By choice of energizing or de-energizing the neutron spin flipper and/or the ^{3}He adiabatic fast passage (AFP) nuclear magnetic resonance (NMR) based flipper, one can measure up to four spin-dependent scattering cross sections, $I^{\rm uu}$, $I^{\rm du}$, and $I^{\rm ud}$, $I^{\rm dd}$, where the first (second) index refers to the initial (final) neutron spin state and the u (d) symbol corresponds to the UP (DOWN) state of a neutron spin. The four microscopic differential spin-dependent scattering cross sections from the sample are defined as $\sigma^{\rm uu}$,$\sigma^{\rm du}$, $\sigma^{\rm ud}$, $\sigma^{\rm dd}$ accordingly. For soft matter samples without any magnetism, $\sigma^{\rm uu}$ is equal to $\sigma^{\rm dd}$ and $\sigma^{\rm ud}$ is equal to $\sigma^{\rm du}$. The measurements were done with the ^{3}He polarization UP. The measured intensities $I^{\rm uu}_{\rm SAM}$ and $I^{\rm du}_{\rm SAM}$ contain small leakages from each imperfect polarizing device. By ray-tracing all possible neutron spin configurations after each polarizing device, $I^{\rm uu}_{\rm SAM}$ and $I^{\rm du}_{\rm SAM}$ can be expressed as

$$\begin{aligned} I^{\rm uu}_{\rm SAM} &= \left(\frac{1+P_{\rm SM}}{2}T^{+}_{\rm SAM,uu}+\frac{1-P_{\rm SM}}{2}T^{-}_{\rm SAM,uu}\right)\left(\sigma^{\rm uu}_{\rm SAM}+T_{\rm S}\sigma^{\rm uu}_{\rm EMP}\right) \\ &+\left(\frac{1+P_{\rm SM}}{2}T^{-}_{\rm SAM,uu}+\frac{1-P_{\rm SM}}{2}T^{+}_{\rm SAM,uu}\right)\left(\sigma^{\rm du}_{\rm SAM}+T_{\rm S}\sigma^{\rm du}_{\rm EMP}\right)+(1-T_{\rm S})\,BGD \end{aligned} \tag{3}$$

$$\begin{aligned} I^{\rm du}_{\rm SAM} &= \left[\frac{1-(2\epsilon-1)P_{\rm SM}}{2}T^{+}_{\rm SAM,du}+\frac{1+(2\epsilon-1)P_{\rm SM}}{2}T^{-}_{\rm SAM,du}\right]\left(\sigma^{\rm uu}_{\rm SAM}+T_{\rm S}\sigma^{\rm uu}_{\rm EMP}\right) \\ &+\left[\frac{1-(2\epsilon-1)P_{\rm SM}}{2}T^{-}_{\rm SAM,du}+\frac{1+(2\epsilon-1)P_{\rm SM}}{2}T^{+}_{\rm SAM,du}\right]\left(\sigma^{\rm du}_{\rm SAM}+T_{\rm S}\sigma^{\rm du}_{\rm EMP}\right)+(1-T_{\rm S})\,BGD \end{aligned} \tag{4}$$

where $T_{\rm S}$ is the transmission of the sample. BGD is the measured beam blocked background of the instrument. $P_{\rm SM}$ is the polarizing efficiency of the supermirror polarizer. The subscripts in scattering cross sections either measured or spin-analyzed refer to either the sample run (SAM) or the empty run (EMP) similar to the routine unpolarized SANS measurements[19]. The subscripts in transmissions (T^+ or T^-) of the ^{3}He analyzer refer to spin configurations (uu or du).

The solution to Eqs. 3 and 4 is

$$\begin{aligned} \left(\sigma^{\rm uu}_{\rm SAM}+T_{\rm S}\sigma^{\rm uu}_{\rm EMP}\right) &= \frac{T^{11}_{\rm SAM}(I^{\rm uu}_{\rm SAM}-BGD)-T^{01}_{\rm SAM}(I^{\rm du}_{\rm SAM}-BGD)}{T^{00}_{\rm SAM}T^{11}_{\rm SAM}-T^{01}_{\rm SAM}T^{10}_{\rm SAM}} \\ \left(\sigma^{\rm du}_{\rm SAM}+T_{\rm S}\sigma^{\rm du}_{\rm EMP}\right) &= \frac{-T^{10}_{\rm SAM}(I^{\rm uu}_{\rm SAM}-BGD)+T^{00}_{\rm SAM}(I^{\rm du}_{\rm SAM}-BGD)}{T^{00}_{\rm SAM}T^{11}_{\rm SAM}-T^{01}_{\rm SAM}T^{10}_{\rm SAM}} \end{aligned} \tag{5}$$

where $T^{00}_{\rm SAM}$, $T^{01}_{\rm SAM}$, $T^{10}_{\rm SAM}$, and $T^{11}_{\rm SAM}$ are given as

$$\begin{aligned} T^{00}_{\rm SAM} &= \frac{1}{2}\left((1+P_{\rm SM})T^{+}_{\rm SAM,uu}+(1-P_{\rm SM})T^{-}_{\rm SAM,uu}\right) \\ T^{01}_{\rm SAM} &= \frac{1}{2}\left((1+P_{\rm SM})T^{-}_{\rm SAM,uu}+(1-P_{\rm SM})T^{+}_{\rm SAM,uu}\right) \\ T^{10}_{\rm SAM} &= \frac{1}{2}\left[(1-(2\epsilon-1)P_{\rm SM})\,T^{+}_{\rm SAM,du}+(1+(2\epsilon-1)P_{\rm SM})\,T^{-}_{\rm SAM,du}\right] \\ T^{11}_{\rm SAM} &= \frac{1}{2}\left[(1-(2\epsilon-1)P_{\rm SM})\,T^{-}_{\rm SAM,du}+(1+(2\epsilon-1)P_{\rm SM})\,T^{+}_{\rm SAM,du}\right] \end{aligned} \tag{6}$$

Similarly the solution to $\sigma^{\rm uu}_{\rm EMP}$ and $\sigma^{\rm du}_{\rm EMP}$ for the empty run is

$$\sigma^{\mathrm{uu}}_{\mathrm{EMP}} = \frac{T^{11}_{\mathrm{EMP}}(I^{\mathrm{uu}}_{\mathrm{EMP}} - BGD) - T^{01}_{\mathrm{EMP}}(I^{\mathrm{du}}_{\mathrm{EMP}} - BGD)}{T^{00}_{\mathrm{EMP}}T^{11}_{\mathrm{EMP}} - T^{01}_{\mathrm{EMP}}T^{10}_{\mathrm{EMP}}}$$
$$\sigma^{\mathrm{du}}_{\mathrm{EMP}} = \frac{-T^{10}_{\mathrm{EMP}}(I^{\mathrm{uu}}_{\mathrm{EMP}} - BGD) + T^{00}_{\mathrm{EMP}}(I^{\mathrm{du}}_{\mathrm{EMP}} - BGD)}{T^{00}_{\mathrm{EMP}}T^{11}_{\mathrm{EMP}} - T^{01}_{\mathrm{EMP}}T^{10}_{\mathrm{EMP}}} \quad (7)$$

Eqs. 5 and 7 describe an appropriate procedure in order to adequately determine σ^{uu} and σ^{du} from the sample. After polarization efficiency correction for both the sample and empty run, σ^{uu} and σ^{du} can be placed on an absolute scale using the incident beam flux measurement.

5. Polarized beam calibration

As the polarizing devices have imperfect efficiencies, proper corrections for small leakage of the undesired neutron spin for each polarizing element is necessary for data analysis. The aim of performing beam calibration is to determine the efficiencies of the supermirror polarizer and the neutron spin flipper. We measured four spin-dependent transmissions, $I^{\mathrm{uu}}_{\mathrm{Trans}}$, $I^{\mathrm{du}}_{\mathrm{Trans}}$, $I^{\mathrm{ud}}_{\mathrm{Trans}}$, $I^{\mathrm{dd}}_{\mathrm{Trans}}$. Similar to Eqs. 3 and 4, we can express the four measured transmitted intensities $I^{\mathrm{uu}}_{\mathrm{Trans}}$, $I^{\mathrm{du}}_{\mathrm{Trans}}$, $I^{\mathrm{ud}}_{\mathrm{Trans}}$, $I^{\mathrm{dd}}_{\mathrm{Trans}}$ in terms of the neutron spin leakage of each polarizing device. Then, the efficiencies of the supermirror and flipper can be solved as following:

$$P_{\mathrm{SM}} = \frac{I^{\mathrm{uu}}_{\mathrm{Trans}}\left(T^{+}_{\mathrm{Trans,ud}} + T^{-}_{\mathrm{Trans,ud}}\right) - I^{\mathrm{ud}}_{\mathrm{Trans}}\left(T^{+}_{\mathrm{Trans,uu}} + T^{-}_{\mathrm{Trans,uu}}\right)}{I^{\mathrm{uu}}_{\mathrm{Trans}}\left(T^{+}_{\mathrm{Trans,ud}} - T^{-}_{\mathrm{Trans,ud}}\right) + I^{\mathrm{ud}}_{\mathrm{Trans}}\left(T^{+}_{\mathrm{Trans,uu}} - T^{-}_{\mathrm{Trans,uu}}\right)} \quad (8)$$

$$(2\epsilon - 1) = \frac{I^{\mathrm{dd}}_{\mathrm{Trans}}\left(T^{+}_{\mathrm{Trans,du}} + T^{-}_{\mathrm{Trans,du}}\right) - I^{\mathrm{du}}_{\mathrm{Trans}}\left(T^{+}_{\mathrm{Trans,dd}} + T^{-}_{\mathrm{Trans,dd}}\right)}{P_{\mathrm{SM}}\left[I^{\mathrm{dd}}_{\mathrm{Trans}}\left(T^{+}_{\mathrm{Trans,du}} - T^{-}_{\mathrm{Trans,du}}\right) + I^{\mathrm{du}}_{\mathrm{Trans}}\left(T^{+}_{\mathrm{Trans,dd}} - T^{-}_{\mathrm{Trans,dd}}\right)\right]} \quad (9)$$

where T^{+} and T^{-} are defined above. For this experiment, the polarizing efficiency of the supermirror was determined to be 0.906 ± 0.008 at 7.5Å. This is lower than 0.94, a value that we have typically obtained without a sample and a chopper. The lower polarizing efficiency might be due to use of a larger aperture in front of the supermirror polarizer for higher incident beam intensity and a magnetic motor shaft of the chopper that was necessarily placed near the beam. The flipper efficiency ϵ was determined to be 0.979 ± 0.006. The ^{3}He analyzing efficiency was over 98.5 % through the entire test. The flipping ratio was measured to be 14 at the beginning of the experiment. Neutron spins after the sample were flipped by inverting the ^{3}He polarization of the analyzer using the AFP NMR technique. During each AFP inversion, the ^{3}He polarization loss was previously determined to be 0.003 % using both the NMR and neutron transmission method to monitor the ^{3}He polarization [20]. So we ignored this small loss when performing the polarized beam calibration.

The ^{3}He polarization decays exponentially with a time constant T_1 and $P_{\mathrm{He}}(t) = P^0_{\mathrm{He}} exp\left(-\frac{t}{T_1}\right)$ where P^0_{He} is the ^{3}He polarization at the beginning of the experiment. Accordingly, the polarized neutronic performance (analyzing efficiency and transmission of the ^{3}He analyzer, instrumental flipping ratio) changed with time, hence it is necessary to correct these time-dependent efficiencies and transmissions. To characterize T_1, we determined the ^{3}He polarizations at regular time intervals by measuring the neutron transmission of the polarized ^{3}He cell with unpolarized neutrons using Eq. 2. The opacity of the cell was determined to be 2.94 ± 0.02. During the experiment, T_1 was determined to be (224 ± 8) h.

6. results

We began with unpolarized measurements for the combined sample of silver behenate powder ($CH_3(CH_2)_{20}COOAg$) back filled with 1 mm-thick light water. Silver behenate powder has been used as a SANS wavelength calibration method where the first three diffraction peaks can be seen in the SANS instrument [21]. The silver behenate sample had a small NSI background from hydrogen along with the diffraction peaks [21]. Light water is a strong NSI scatterer. The combined silver behenate and water sample contained diffraction peaks as well as a significant nearly Q-independent NSI background. SANS polarization analysis was used to separate the coherent scattering from NSI scattering. The water sample was added to test our ability to remove a strong NSI signal from measured small angle scattering. For a direct comparison with the polarized beam experiment using a chopper, the unpolarized measurements were carried out using the same experimental setup as that used in the polarized measurements. The unpolarized data for the combined sample were corrected for background, detector efficiency, empty sample cell holder, and sample transmission using the SANS software [19]. The data were placed on an absolute scale using the direct beam flux measurement. The presence of the magnetically shielded solenoid and choice of 7.5 Å limited by the chopper allowed us to observe the first diffraction peak only as shown in Fig. 2. The data, radially averaged and on an absolute scale, are shown in Fig. 3. The first diffraction peak is located at 0.1076 $Å^{-1}$, as expected.

Polarized measurements with the chopper were performed for the non-spin-flip (UU) and spin-flip (DU) scattering with and without the chopper as discussed in the data reduction section. As depicted in Sec. 4, polarized data were corrected for background, detector efficiency and time-dependent transmission and polarization efficiency of the ^{3}He analyzer. Again, the data were also placed on an absolute scale using the direct beam flux measurement. Small-angle scattering from the ^{3}He glass container contributes an additional background and has been measured to be approximately Q-independent for the Q range interested here [17]. This was properly subtracted as shown in the reference [4]. This procedure was applied for the sample and empty

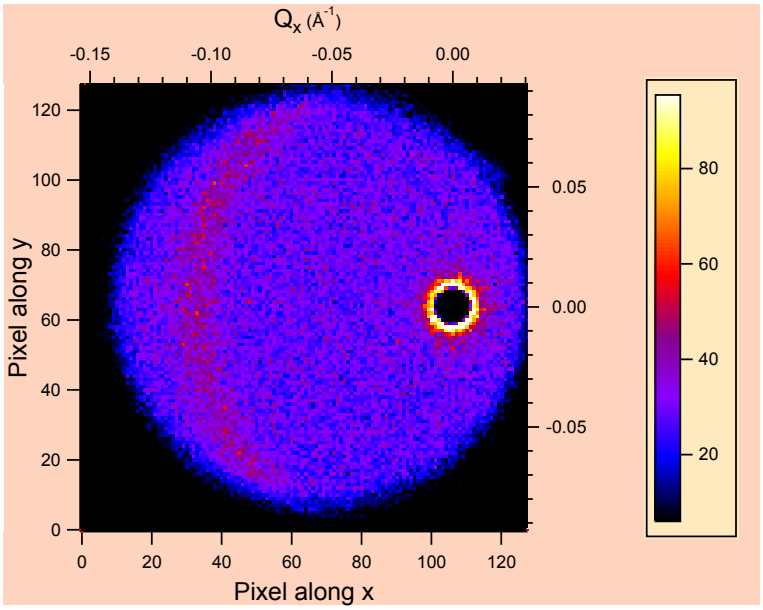

Figure 2. Color online. SANS image for the unpolarized measurements for silver Behenate powder back filled with light water. The large circle indicates the Q limit from the neutron shielding material attached to the mu-metal end cap hole of the magnetically shielded solenoid.

run separately. It has been reported that 1 mm-thick light water produced a significant inelastic scattering [14, 15]. With the chopper in the polarized beam configuration, polarization analysis can be done with options of either ignoring the inelastic data (elastic data only) or using both elastic and inelastic data. The latter is what has been demonstrated before [3] for a sample where inelastic scattering was ignored and multiple scattering was small. In both configurations shown in Fig. 3, σ^{du} is nearly Q-independent from part of spin-incoherent scattering and σ^{uu} shows a diffraction peak at 0.1076 $\mathrm{\AA}^{-1}$ as well as a nearly Q-independent spin-incoherent scattering background. The height and width of the diffraction peak with polarization analysis are the same as those from unpolarized measurements. However, both σ^{uu} and σ^{du} determined with only the elastic component yield a reduced spin-incoherent scattering component due to removal of the inelastic background.

For a hydrogen-containing soft matter sample using the SANS configuration shown in Fig. 1,

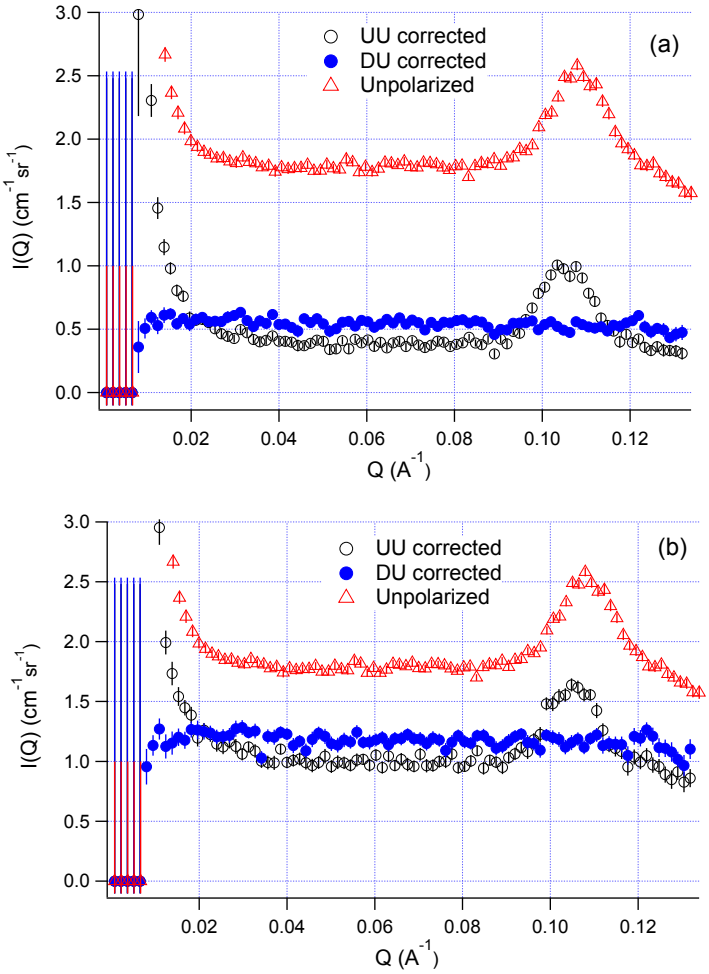

Figure 3. Color online. Polarization efficiency corrected, radially averaged data on an absolute scale ($\mathrm{cm}^{-1}\mathrm{sr}^{-1}$) for a sample of 0.5 mm-thick silver behenate back filled with 1 mm-thick light water for (a) the elastic data only and (b) both elastic and inelastic data. Non spin-flip data σ^{uu} are shown in black open circles; spin-flip data σ^{du} are shown in blue solid circles. Unpolarized data (red open triangles) are also shown for comparison. All uncertainties given in the paper represent one standard deviation.

two-thirds of nuclear spin-incoherent scattering ($\sigma_{\rm NSI}$) shows in the spin-flip (SF) channel and one-third shows in the non-spin flip (NSF) channel. As stated previously, the measured non-spin-flip signal contains both coherent scattering ($\sigma_{\rm Coh}$) and $\frac{1}{3}$ of spin-incoherent scattering. However, the ratios of $\frac{1}{3}$ and $\frac{2}{3}$ of the NSI scattering to the NSF and SF channels will not hold true if there is a significant fraction of multiple scattering events from the hydrogen-containing sample. Neutrons that scatter twice contribute $\frac{5}{9}$ and $\frac{4}{9}$ of the NSI scattering to the NSF and SF channel, respectively; Neutrons that scatter three (four) times contribute $\frac{13}{27}$ ($\frac{41}{81}$) and $\frac{14}{27}$ ($\frac{40}{81}$) of the NSI scattering to the NSF and SF channel, respectively and so on. The multiple scattering in such a sample effectively decreases the two-to-one ratio of the SF channel to NSF channel of the NSI scattering, approaching an one-to-one ratio. Assuming that the probability of the spin flip scattering in the total NSI scattering is p ($0.5 \leq p \leq \frac{2}{3}$), the measured non-spin flip scattering $\sigma^{\rm uu}_{\rm SAM}$ and spin-flip scattering $\sigma^{\rm du}_{\rm SAM}$ can be expressed as

$$\sigma^{\rm uu}_{\rm SAM} = \sigma_{\rm Coh} + (1-p)\sigma_{\rm NSI} \tag{10}$$

$$\sigma^{\rm du}_{\rm SAM} = p\sigma_{\rm NSI} \tag{11}$$

To estimate the effect of multiple scattering to the spin flip scattering for 1 mm-thick light water with a measured transmission of 0.5, we have done Monte-Carlo simulation where no inelastic scattering is assumed in the scattering kernel. The Monte-Carlo simulation has been

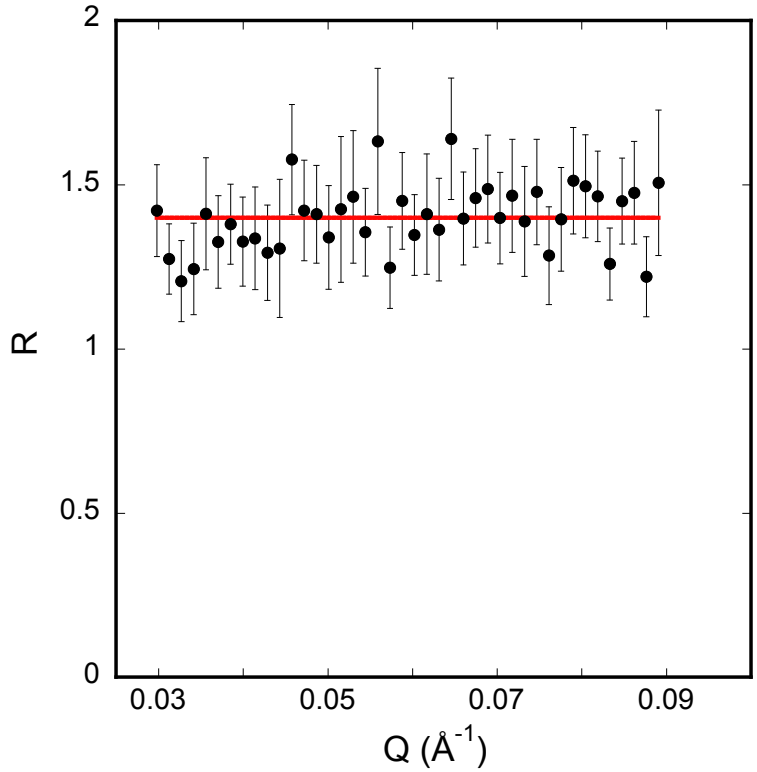

Figure 4. Color online. Ratio R ($R = \frac{\sigma^{\rm du}}{\sigma^{\rm uu}}$) in the Q range from 0.03 Å to 0.09 Å where coherent scattering is negligible. $\sigma^{\rm uu}$ and $\sigma^{\rm du}$ were polarization efficiency corrected with the elastic data. The ratio was fit to a constant, $\frac{p}{1-p}$. p is determined to be 0.583 ± 0.005, agreeing with the Monte Carlo simulation discussed in the text.

thoroughly described in the references [15, 22]. We found that the ratio $\frac{I_{n+1}}{I_n}$ of the intensity of successive orders of multiple scattered neutrons is 0.45. Here I_n is the intensity of neutrons that have been scattered n times. This agrees with the model in the reference [23]. From the Monte-Carlo simulation, we determined p to be 0.58. p can also be determined by fitting the ratio R of $\sigma_{\rm SAM}^{\rm du}$ to $\sigma_{\rm SAM}^{\rm uu}$ to a constant in the Q range from 0.03 Å^{-1} to 0.09 Å^{-1} where coherent scattering is negligible. The fitted constant is equal to $\frac{p}{1-p}$. Fig. 4 shows R versus Q. We found $R = 1.4$ and $p = 0.583 \pm 0.005$, which agrees well with the Monte-Carlo simulation. For samples that exhibit minimal multiple scattering, R would be close to 2 and p would be close to 0.667. Using Eqs. 10 and 11 and the determined value of p, the coherent scattering from silver behenate can be separated from the strong nuclear spin-incoherent scattering in the NSF channel. The results are shown in Fig. 5 for the elastic data (Fig. 5(a)) and for both the elastic and inelastic data (Fig. 5(b)). As a comparison, the unpolarized data are also shown. As expected, the nuclear spin-incoherent scattering background obtained from the elastic data is smaller than that from unpolarized measurements due to removal of the inelastic scattering.

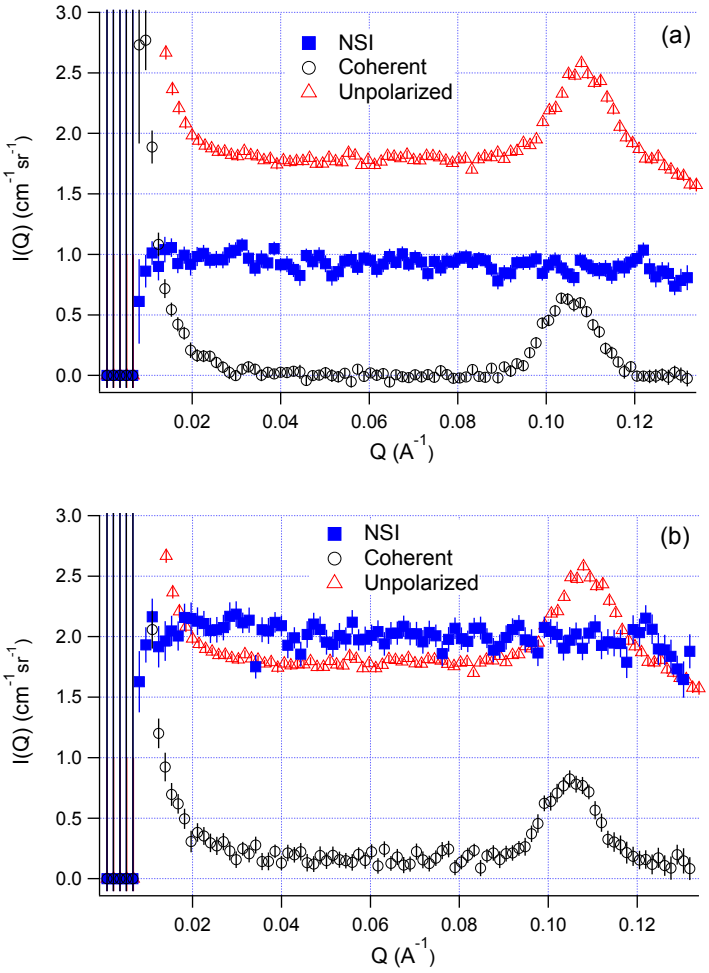

Figure 5. Color online. Separation of coherent scattering $\sigma_{\rm Coh}$ (black open circles) from nuclear spin-incoherent scattering $\sigma_{\rm NSI}$ (blue solid boxes) for a sample of 0.5 mm-thick silver behenate back filled with 1 mm-thick light water for (a) the elastic data only and (b) both elastic and inelastic data. Unpolarized data (red open triangles) are also shown for comparison.

However, the nuclear spin-incoherent scattering obtained using both elastic and inelastic data is higher than that from unpolarized measurements, leading to an unphysical result. Also σ_{Coh} has a residual nearly Q-independent background. This is because the inelastic scattering occurs at different wavelengths with a peak at 1.4 Å [15]. The polarizing efficiency and transmissions of the ^{3}He analyzer are strongly wavelength-dependent. We had an initial ^{3}He polarization of 0.81 during the test, which provided an analyzing efficiency of 0.983 and transmission of 0.496 for the desired spin state at 7.5 Å. This would be 0.417 for the analyzing efficiency and 0.784 for the transmission at 1.4 Å. Therefore, for hydrogen-containing soft matter samples that exhibit both inelastic scattering and nuclear spin-incoherent scattering, the general polarization analysis method [3] may not be adequate for separation of coherent scattering from NSI scattering without the time-of-flight technique to remove the inelastic scattering. If the sample exhibits multiple scattering, the effect of multiple scattering to polarized beam performance has to be taken into account.

To estimate whether there is any improvement in the determined signal-to-noise (S/N) ratio of coherent scattering using the method of polarization analysis combined with TOF, we assume that the uncertainty is due solely to Poisson counting statistics. As shown in Fig. 3(a), the nearly Q-independent background for polarization analysis with TOF is reduced by a factor of 4.5 compared with that from the normal unpolarized SANS measurement. During the experiment, the reduction in count rate was a factor of 6 from the chopper with a duty cycle of 16.7 %, and a factor of 5.5 from the supermirror polarizer and the ^{3}He analyzer. Hence the overall reduction in count rate from polarization analysis with TOF was a factor of 33. The factor of 4.5 improvement in the S/N ratio shown in Fig. 3(a) is cancelled by the factor of 33 reduction in count rate from polarization analysis with TOF. We have installed a superemirror polarizer with a higher polarization efficiency and transmission. The chopper could be operated at a duty cycle of 25 %. In the future, a ^{3}He polarization of 90 % may be achievable [24], resulting in a higher polarization efficiency and transmission for the ^{3}He analyzer. The overall reduction in count rate from polarization analysis with TOF would be a factor of 14. The improvement using polarization analysis with TOF would be still limited compared with a normal unpolarized SANS measurement. For a normal unpolarized SANS measurement for biological macromolecule samples, it is necessary to carefully prepare addition samples such as dilute solution to determine the Q-independent background [1]. However it does not require such a necessity using polarization analysis with TOF. In addition, the Q-independent background can not always be observed at large Q for certain hydrogen-rich samples. A Q-dependence of the measured SANS signal for the large molecular size of the alkines has been reported [25]. In this case, SANS polarization analysis combined with the time-of-flight technique can be used to separate coherent scattering from spin-incoherent scattering, hence offering a different approach to obtain the correct structural information without a need to determine the background accurately.

7. Conclusions

We have done polarization analysis with the time-of-flight technique using a chopper that was used to effectively remove the inelastic background for a sample of 0.5 mm-thick silver behenate back filled with 1 mm-thick light water. We have developed a data reduction procedure for SANS polarization analysis in conjunction with the time-of-flight technique. With such a setup, proper data reduction and the Monte Carlo simulation for multiple scattering estimation, we have unambiguously separated the first diffraction peak of silver behenate from the strong spin-incoherent background for a sample of silver behenate back filled with 1 mm-thick light water that is known to exhibit strong nuclear spin-incoherent scattering, inelastic scattering and multiple scattering. We show that the SANS polarization analysis method without an appropriate correction to inelastic scattering using the time-of-flight technique may not be

adequate to separate coherent scattering from spin-incoherent scattering for samples that show inelastic scattering. Polarization analysis combined with the time-of-flight technique reduced Q-independent background from hydrogen by a factor of 4.5 compared with a normal unpolarized SANS measurement for the sample of 0.5 mm-thick silver behenate back filled with 1 mm-thick light water. The factor of 4.5 improvement in the signal-to-noise ratio is cancelled by the factor of 33 reduction in count rate from polarization analysis with TOF. However, for samples where the Q-independent background can not observed at large Q, SANS polarization analysis in conjunction with the time-of-flight technique offers a different approach to determine the structural information from coherent scattering.

Acknowledgments

The authors thank J. Anderson, J. Fuller, and A. Kirchhoff of the NIST Optical Shop for assistance with cell fabrication. We benefitted in using the Monte Carlo simulation code written by Gordon Jones. The work utilized facilities supported in part by the National Science Foundation under Agreement No. DMR-1508249.

References

[1] Rubinson, K. A., stanley, C., & Krueger, S., (2008) *J. Appl. Cryst.*, **41**, 456-465.
[2] Moon, R., Riste, T., Koehler, W., (1969) *Phys. Rev.*, **181**, 920931.
[3] Gentile, T. R., Jones, G. L., Thompson, A. K., Barker, J., Glinka, C. J., Hammouda, B., and Lynn, J. W. (2000) *J. Appl. Cryst.*, **33**, 771-774.
[4] Krycka, K. L., Booth, R. A., Borchers, J. A., Chen, W. C., Conlon, C., Gentile, T. R., Hogg, C., Ijiri, Y., Laver, M., Maranville, B. B., Majetich, S. A., Rhyne, J., and Watson, S. M., (2009) *Physica B*, **404**, 2561-2564.
[5] Chen, W. C., Erwin, R., McIver, J. W. III, Watson, S., Fu, C. B., Gentile, T. R., Borchers, J. A., Lynn, J. W., and Jones, G. L. (2009) *Physica B*, **404**, 2663-2666.
[6] Krycka, K. L., Chen, W. C., Borchers, J. A., Maranville, B. B., Watson, S. M., (2012) *J. Appl. Cryst.*, **45(3)**, 546-553.
[7] Krycka, K. L., Booth, R. A., Hogg, C. R., Ijiri, Y., Borchers, J. A., Chen, W.C., Watson, S.M., Laver, M., Gentile, T.R., Dedon, L. R., Harris, S., Rhyne, J. J., and Majetich, S.A., (2010) *Phys. Rev. Lett.*, **104**, 207203; Krycka, K. L., Borchers, J. A., Ijiri, Y., Hasz, K., Rhyne, J. J., Booth, R. A., and Majetich, S.A., (2014) *Phys. Rev. Lett.*, **113**, 147203.
[8] Dufour, C., Fitzsimmons, M. R., Borchers, J. A., Laver, M., Krycka, K. L., Dumesnil, K., Watson, S. M., Chen, W. C., Won, J., Singh, S., (2011) *Phys. Rev. B*, **84**, 064420.
[9] Ramazanoglu, M., Laver, M., Ratcliff, W., Watson, S. M., Chen, W. C., Jackson, J., Kothapalli, J., Seongsu, L, Cheong, S. -W., and Kiryukhin, V., (2011) *Phys. Rev. Lett.*, **107**, 207206 (2011).
[10] Laver, M., Mudivarthi, C., Cullen, J. R., Flatau, A. B., Chen, W. C., Watson, S. M., and Wuttig, M., (2010) *Phys. Rev. Lett.*, **105**, 027202.
[11] Gaspar, A. M., Busch, S., Appavou, M. -S., Haeussler, W., Georgii, R., Su, Y., and Doster, W., (2010) *Biochim. Biophys. Acta*, **1804**, 76-82.
[12] Ioffe, A., Babcock, E., Pipich, V., Radulescu, A., (2011) *J. Phys.: Conf. Series*, **294**, 012013.
[13] Babcock, E., Salhi, Z., Appavou, M-S., Feoktystov, A., Pipich, V., Radulescu, A., Ossovyi, V., staringer, S., and Ioffe, A.,(2013) *Phys. Procedia*, **42**, 154-162.
[14] Ghosh, R. E., Rennie, A. R., (1999) *J. Appl. Cryst.*, **32**, 1157-1163.
[15] Barker, J. G., Mildner, D. F. R., (2015) *J. Appl. Cryst.*, **48**, 1055-1071 and references therein.
[16] GE Lighting Component Sales, Bldg. 315D, 1975 Noble Rd., Cleveland, OH 44117. Certain trade names and company products are mentioned in the text or identified in an illustration in order to adequately specify the experimental procedure and equipment used. In no case does such identification imply recommendation or endorsement by the National Institute of Standards and Technology, nor does it imply that the products are necessarily the best available for the purpose.
[17] Chen, W. C., Gentile, T. R., O'Donovan, K. V., Borchers, J. A., and Majkrzak, C. F., (2004) *Rev. Sci. Instrum.*, **75**, 3256-3263.
[18] Chen, W. C., Gentile, T. R., Erwin, R., Watson, S.M., Ye, Q., Krycka, K.L., and Marvanville, B.B., (2014) *J. Phys.: Conf. Ser.* **528** 012014
[19] Kline, S. R. (2006) *J. Appl. Cryst.*, **39(6)**, 895.

[20] Optimization of the ^{3}He spin inversion by the AFP NMR method is not important for this test, so will not be discussed in details here and will be published elsewhere.
[21] Gilles, R., Keiderling, U., Wiedermann, A., (1998) *J. Appl. Cryst.*, **31**, 957-959.
[22] Barker, J. G., unpublished.
[23] Mayers, J., & Cywinski, R., (1985) *Nucl. Instr. and Meth.*, **241**, 519531.
[24] We have recently achieved a ^{3}He polarization of 89 %.
[25] Arleth, L., Pedersen, J. S., (2000) *J. Appl. Cryst.*, **33**, 650-652